ORIGINAL RESEARCH

Neurovascular Imaging with Ultra-High-Resolution Photon-Counting CT: Preliminary Findings on Image Quality Evaluation

Adrienn Tóth, Justin A. Chetta, Milad Yazdani, M. Gisele Matheus, Jim O 'Doherty, Sameer V. Tipnis, M. Vittoria Spampinato

ABSTRACT

BACKGROUND AND PURPOSE: The first-generation photon-counting detector (PCD) CT was recently introduced into clinical practice and represents a promising innovation in high-resolution CT imaging. The purpose of this study was to assess the image quality of ultra-high-resolution (UHR) PCD-CT compared with energy-integrating detector (EID)-CT, and to explore different reconstruction kernel sharpness levels for the evaluation of intracranial aneurysms.

MATERIALS AND METHODS: Ten patients with intracranial saccular aneurysms, who had previously undergone conventional EID-CT, were prospectively enrolled. CT angiograms were acquired on a clinical dual-source PCD-CT in UHR mode, and reconstructed with four vascular kernels (Bv36, Bv40, Bv44, Bv48). Quantitative and qualitative image quality parameters of the intracranial arteries were evaluated. For the quantitative analysis (image noise, SNR, CNR), regions of interest were manually placed at standard anatomical intracranial and extracranial locations by one author. In addition, vessel border sharpness was evaluated quantitatively. For the qualitative analysis, three blinded neuroradiologists rated PCD-CT and EID-CT image quality for the evaluation of the intracranial vessels (i.e., the aneurysms and nine standard vascular branching locations) on a 5-point Likert-type scale. Additionally, readers independently selected their preferred kernel among the four kernels evaluated on PCD-CT.

RESULTS: In terms of quantitative image quality, Bv48, the sharpest kernel, yielded increased image noise, and decreased SNR and CNR parameters compared to Bv36, the smoothest kernel. Compared to EID-CT, the Bv48 kernel offered better quantitative image quality for the evaluation of small intracranial vessels ($p < .001$). Image quality ratings of the Bv48 were superior to those of the EID-CT, and not significantly different from ratings of the B44 reconstruction kernel. When comparing side-by-side all four PCD-CT reconstruction kernels, readers selected the B48 kernel as the best to visualize the aneurysms in 80% of cases.

CONCLUSIONS: UHR PCD-CT provides improved image quality for neurovascular imaging. Although the less sharp kernels provided superior SNR and CNR, the sharpest kernels delivered the best subjective image quality on PCD-CT for the evaluation of intracranial aneurysms.

ABBREVIATIONS: CNR = Contrast-to-Noise Ratio; EID-CT = Energy-Integrating Detector CT; PCD-CT = Photon-Counting Detector CT; QIR = Quantum Iterative Reconstruction; UHR = Ultra-High-Resolution.

Received February 12, 2024; accepted after revision May 07, 2024.
From the Department of Radiology and Radiological Science (A.T., J.A.C., M.Y., M.G.M., J.O.D., S.V.T., M.V.S.), Medical University of South Carolina, Charleston, SC, United States; and Siemens Medical Solutions (J.O.D.), Malvern, PA, United States.

M. V. Spampinato has been the recipient of research funding from Siemens and from the Medical University of South Carolina Office of Innovation. J. O'Doherty is an employee of Siemens Medical Solutions USA, Inc.

Please address correspondence to M. Vittoria Spampinato, MD, Department of Radiology and Radiological Science, Medical University of South Carolina, 96 Jonathan Lucas Street, Charleston, SC 29425, United States; spampin@musc.edu.

SUMMARY SECTION

PREVIOUS LITERATURE: Sharper reconstruction kernels in CT angiography can enhance spatial frequencies and image detail, approaching the image quality achieved by 3D angiography, and show promise for improving clinical decision-making by providing more accurate anatomical characterization of intracranial aneurysms. While previous studies have evaluated ultra-high-resolution photon-counting CT for coronary angiography and recommended optimal kernel selection, there is a lack of literature on its use in neurovascular imaging.

KEY FINDINGS: The use of the Bv48 kernel significantly improved vessel sharpness, especially in smaller intracranial arteries. The three readers of the study favored the sharper kernels for the visualization of saccular aneurysms. UHR PCD-CT images significantly improved vessel sharpness and subjective image quality compared to standard EID-CT.

KNOWLEDGE ADVANCEMENT: This study provides an initial evaluation of objective and subjective image quality using four different reconstruction kernels in a selected group of patients with intracranial saccular aneurysms. Our preliminary results could lay the foundation for future studies and help guide protocol optimization for neurovascular imaging with PCD-CT.

INTRODUCTION

Computed tomography angiography (CTA) is routinely performed to evaluate intracranial aneurysms with high reported sensitivity and specificity.[1-5] However, the spatial resolution of conventional CT (energy-integrating detector CT or EID-CT) is not always adequate to fully characterize small aneurysms (3 mm or less) and may have limitations in differentiating a tortuous vessel or infundibulum from an aneurysm.[6] The recent introduction of photon-counting detectors (PCDs) is a breakthrough in CT technology. Conventional EIDs convert the incoming X-ray photons into visible light, which is then converted into electrical signal. Instead, PCDs omit the light scintillation step, and directly generate electrical signal proportional to the energy of an incoming X-ray. This results in measurement of the energy of the incident photons, thus enabling multi-energy imaging.[7-9] With currently available whole body clinical PCD-CT systems, ultra-high resolution (UHR) imaging is available with a detector pixel size of 0.151 x 0.176 mm2 at the isocenter, offering a maximum in-plane image resolution of 0.11 mm and a maximum through-plane resolution of 0.16 mm.[10] These technical innovations allow for improved soft tissue and iodine contrast, improved spatial resolution, decreased image noise, reduced beam hardening and metal-associated artifact.[11-15] We hypothesize that the enhanced image quality of UHR PCD-CT may facilitate the detailed characterization of intracranial aneurysms. The selection of the reconstruction kernel is a key aspect of image post-processing that requires careful consideration, as it frequently involves striking a balance between enhanced spatial resolution and image noise.[16, 17] As for the detailed anatomic characterization of intracranial aneurysms, sharper kernels may provide more accurate information than smooth CT kernels.[18] In the present study, we aimed to assess the image quality of UHR PCD-CT compared with EID-CT, and to explore different reconstruction kernel sharpness levels for the evaluation of intracranial aneurysms.

MATERIALS AND METHODS

Study Population

This prospective, single-center study was approved by the institutional review board and written informed consent was obtained from all participants. Consecutive patients between July and September 2023 who met the following criteria were enrolled: age 18 years or older, had a prior clinically indicated standard of care (SOC) CTA of the head and neck on EID-CT within the previous six months, and had one or multiple untreated intracranial saccular aneurysms. Exclusion criteria included history of iodine contrast allergy, renal insufficiency, pregnancy, nondiagnostic SOC CTA, and scheduled neurovascular surgery (endovascular coiling or clipping). After the initial screening, the senior author reviewed each CT angiogram to confirm eligibility for the study. If it was unclear whether the patient had a saccular aneurysm or an infundibulum, then the patient was excluded from the study.

PCD-CT Image Acquisition and Reconstruction

Patients underwent head and neck CTA acquired on a clinical first-generation PCD-CT scanner (NAEOTOM Alpha, Siemens Healthineers, Forchheim, Germany) operated in "Quantum HD" ultra-high-resolution (UHR) mode, resulting in a collimation of 120 x 0.2 mm at the detector level and a reconstructed slice thickness of 0.2 mm. The reconstructed matrix size was 512 x 512, and the field of view was adjusted for each patient to optimally image the vessels from the aortic arch to the vertex. The following acquisition parameters were used: tube voltage 140 kVp, pitch 0.65, rotation time 0.5 s. To achieve a comparable absorbed radiation dose between scans, the CT dose index ($CTDI_{vol}$) from the EID-CT scan of each patient was used as a reference. The tube current-time product (mAs) of the PCD-CT scan was adjusted in order to match the reference $CTDI_{vol}$.

CTA was performed after the administration of 80 ml iodinated contrast material (iohexol, Omnipaque 350, GE Healthcare), injected through a 20-gauge intravenous antecubital vein catheter using a power injector. The flow rate was matched to the EID-CT scan per patient, with an average of 4.37 (± 0.5) ml/s. Opacification of the aortic arch was monitored using a bolus tracking technique with an attenuation threshold of 155 HU for all examinations. The start time of data acquisition was determined with a fixed delay of five seconds after the attenuation threshold was reached.

Axial plane, polyenergetic images (referred to as 'T3D' by the manufacturer) were reconstructed at 0.2 mm slice thickness with 0.2 mm slice increment. Iterative reconstruction (denoted "QIR" by the manufacturer) level 1 was used for all PCD-CT images. Four image sets were reconstructed using the following vascular kernels: Bv36 (least sharp, representing the standard clinical reconstruction kernel used for head and neck CTA in our institution), Bv40, Bv44, and Bv48 (Supplementary Table 1).

Quantitative Analysis

Quantitative image analysis was performed by one author (A.T.), using a manufacturer-specific workstation (Syngo.Via, VB30 version, Siemens Healthineers). Regions of interest (ROIs) were manually placed on one PCD-CT reconstruction (Bv36) at 12 standard anatomical locations, bilaterally. ROIs were copied and then pasted onto the other three reconstructions, allowing to place the ROIs at the exact same location with the exact same size on every PCD-CT reconstruction. The ROIs on the EID-CT images were closely matched (manually) in both size and location to the PCD-CT image sets per patient basis. The data analysis utilized the average of the two bilateral ROIs at each location.

Attenuation was measured in three extracranial vessels: the common carotid artery (CCA), the cervical internal carotid artery (ICA, C1), and the cervical vertebral artery (VA, V2). Seven intracranial locations were selected: petrous segment of the ICA (C2), carotid terminus (CT), middle cerebral artery (MCA, M1), anterior cerebral artery (A2), posterior cerebral artery (P2), intradural vertebral artery (V4) and the basilar artery (BA). The size of the ROIs was as large as possible, ensuring that only the contrasted lumen of the artery was measured. Intracranial vessel measurements were divided into two groups based on the size of the ROIs: the first comprised of large intracranial vessels including C2 and CT (ROI area = 4.28 ± 2.02 and 2.39 ± 0.74 mm2, respectively), while the second consisted of small intracranial vessels such as M1, A2, P2, V4, and BA (ROI area ranged from 0.70 ± 0.20 mm2 to 1.53 ± 0.36 mm2). Results from the analysis of the combined groups were reported.

Signal was defined as the average density (Hounsfield units, HU) and noise as the standard deviation (SD) of density within the voxels of the ROIs. For the calculation of the signal-to-noise ratio (SNR) and contrast-to-noise ratio (CNR), the muscle density in the pterygoid

muscle and the standard deviation of the air adjacent to the neurocranium were measured (both ROI areas: 0.25 cm2). SNR and CNR were calculated as follows:

$$SNR = \frac{signal_{artery}}{standard\ deviation_{artery}}$$

$$CNR = \frac{signal_{artery} - signal_{muscle}}{standard\ deviation_{air}}$$

Additionally, images were transferred to a dedicated workstation (ImageJ, version 1.53) to analyze sharpness of vessel borders.[17, 19, 20] For each image, a total of six line profiles were placed perpendicular to the border of the vessels to detect attenuation values at the following locations: C1 and V2 (representing the 'extracranial arteries'), C2 and CT (representing the 'large intracranial arteries'), M1 and A2 (representing the 'small intracranial arteries'). For each line, the maximum per-pixel change in signal intensity (max. ΔHU) and full-width-half-maximum (FWHM) was calculated. Vessel sharpness was defined as the mean maximum change of CT values.

Qualitative Analysis

Qualitative image quality was assessed by three experienced neuroradiologists (J.A.C., M.G.M., and M.Y.). Image analysis was performed using the in-house picture archiving and communication system (Sectra, Linköping, Sweden). A training session was conducted with the readers prior to the image rating and reference images were provided to ensure consistency and facilitate the application of the rating scale. The readers independently rated the images at the following intracranial locations: right and left ICA (C2 segment), posterior inferior cerebellar arteries (PICA), vertebral artery – basilar artery junctions (VB), ophthalmic arteries (OA), CT, posterior communicating artery (PCOM), MCA trifurcation, anterior communicating artery (ACOM), BA apex, and at the location of the aneurysm/s. In the first part of the evaluation, PCD-CT reconstructions and EID-CT images were displayed one by one sequentially in a randomized order, while readers were asked to rate the image quality using a 5-point Likert-type scale (Supplementary Table 2). Images were initially shown at predefined window settings (width: 1500 HU; level: 400 HU), but the readers were allowed to perform manual adjustment. Next, the four PCD-CT reconstructions of each patient were displayed on one monitor in a randomized order and readers were asked to choose the most suitable for the evaluation of the intracranial aneurysm/s. Readers were blinded to the type of the reconstructions and scanner type at each step of the image evaluation.

Statistical Analysis

Patient and examination characteristics were summarized descriptively. Normality of distributions was assessed using histograms and the Shapiro-Wilk test. The two-sided Wilcoxon signed-rank test were used to assess differences in the distribution of qualitative and non-normally distributed quantitative image quality scores. Scores from the qualitative image quality analysis were pooled across readers. The inter-reader agreement of qualitative scores among the three readers was quantified with Krippendorf's α coefficients (α = 0.0 – 0.20; poor agreement, α = 0.21 – 0.40; fair agreement, α = 0.41 – 0.60; moderate agreement, α = 0.61 – 0.80; substantial agreement, α = 0.81 – 1.00; almost perfect agreement). All p values were corrected for multiple testing using the Bonferroni correction. Two-tailed p-values less than 0.05 were considered statistically significant. If not stated otherwise, all data are presented as mean ± standard deviation (SD). All statistical analyses were performed using IBM, SPSS, version 28.0.1.

RESULTS

Patient Population and Radiation Dose Parameters

Example images are provided in Figure 1. The study population included ten patients, and eight were women. Mean age at the time of the second (PCD-CT) scan was 59.5 (± 18.3) years. The indications of the SOC CTA included aneurysm follow-up or sudden headache with a history of intracranial aneurysm (n= 6), clinical suspicion of acute stroke (n=2), head trauma (n=1), dizziness (n=1). A total of 13 intracranial aneurysms were detected at the following locations: ICA (n=5), MCA (n=4), ACOM (n=2), PCOM (n=2), with an average maximum diameter of 3.5 (± 1.5) mm (Supplementary Table 3). Radiation dose parameters for the EID-CT and PCD-CT examinations were as follows: CTDIvol 22.55 (±12.16) mGy, DLP 695.35 (±288.58) mGy*cm, effective mAs 270.22 (±55.65) and CTDIvol 18.87 (± 3.03) mGy, DLP 695.50 (±127.03) mGy*cm, effective mAs 175.70 (±35.36), respectively.

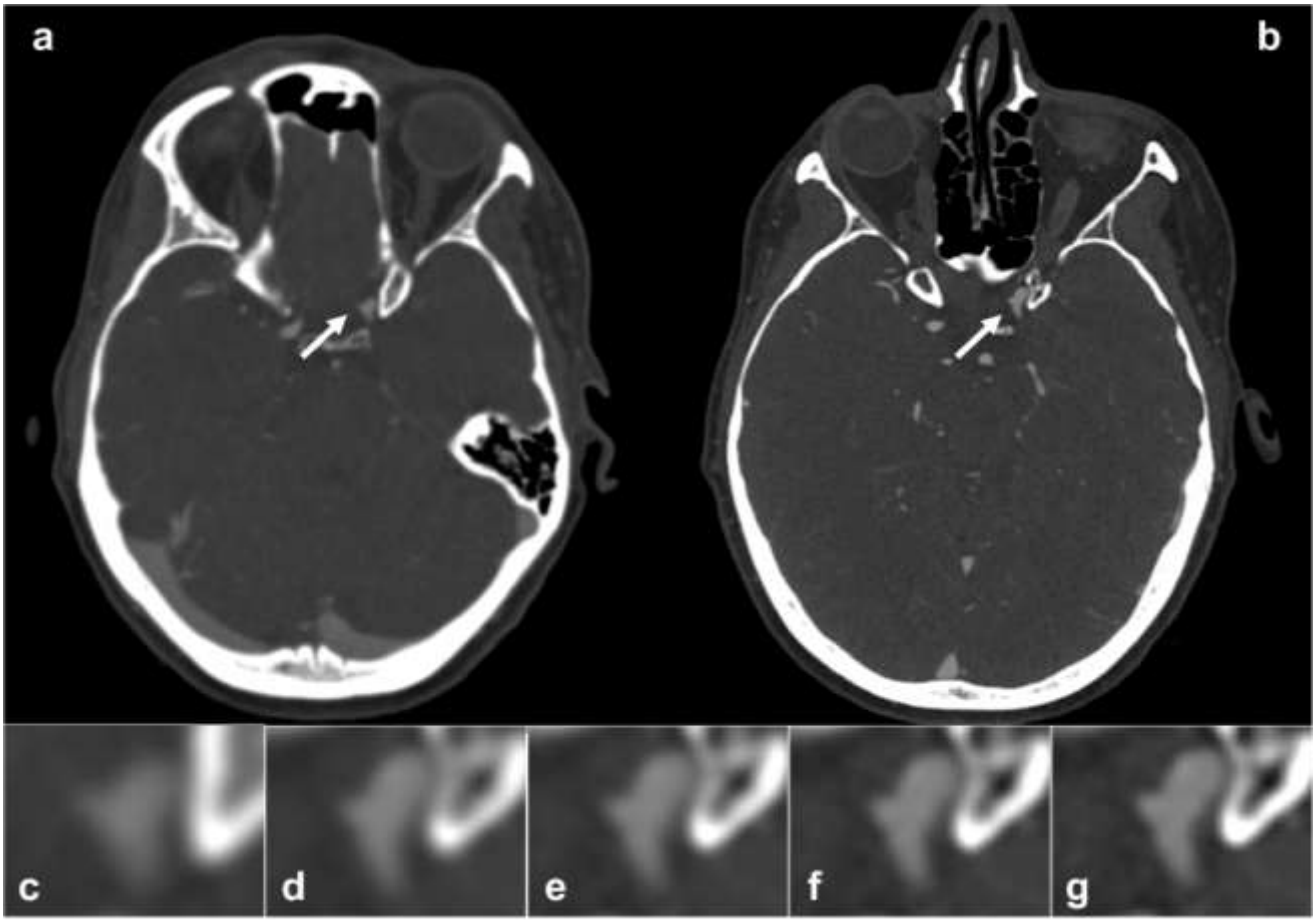

FIG 1. 44-year-old female with saccular intracranial aneurysm. EID-CT (a and c) and UHR PCD-CT (b, d-g) angiography images of the head show intracranial saccular aneurysm of the left paraclinoid ICA (arrows). PCD-CT reconstructions show increasing vessel sharpness with higher kernel levels: d (Bv36), e (Bv40), f (Bv44), g (Bv48). Window settings were identical in each image. (Bv = Body vascular, EID-CT = Energy-integrating detector CT, ICA = Internal Carotid Artery, PCD-CT = Photon-counting detector CT, UHR = Ultra-High-Resolution)

Quantitative Analysis – PCD-CT Reconstructions

An incremental increase in attenuation was found across the range of kernels, transitioning from the smoothest (Bv36) to the sharpest (Bv48) kernel in the extracranial (from 516.13 ± 108.1 to 521.92 ± 108.53, respectively) and large intracranial (from 476.88 ± 104.70 to 489.38 ± 106.88, respectively) locations, and a more pronounced increase was evident in the small intracranial arteries (from 425.74 ± 91.21 to 482.23 ± 110.89, respectively) (all from $p < .001$ to $p = .048$). Image noise significantly increased from Bv36 to Bv48, with the highest increase measured at the large intracranial vessels (from 10.70 ± 2.69 to 19.25 ± 3.62, $p < .001$). The least sharp kernel (Bv36) provided the highest SNR and CNR, mostly with significant differences compared to the sharpest (Bv48) kernel (from $p < .001$ to $p = .228$). Vessel sharpness increased with higher kernel levels ($p < .001$) with the greatest difference observed in small intracranial vessels (from 139.87 ± 31.23 to 221.69 ± 49.46) (Figures 2-3 and Supplementary Table 4).

Quantitative Analysis – PCD-CT vs EID-CT

Quantitative image quality measures from EID-CT and PCD-CT (Bv48) were compared. Vascular attenuation as measured on PCD-CT reconstructions was significantly higher than that of EID-CT at each location (from $p < .001$ to $p = .004$). While there was no statistically significant difference in image noise between the PCD-CT Bv48 images and EID-CT at the extracranial and large intracranial locations ($p=.224$ and $p=.646$, respectively), the Bv48 reconstruction exhibited significantly lower image noise in the small intracranial arteries (16.66 ± 4.96 vs 19.95 ± 7.04, $p=.012$). In terms of SNR and CNR, PCD-CT outperformed the EID-CT images at every location, with a statistically significant difference at the small intracranial arteries (30.65 ± 8.86 and 27.76 ± 8.71 vs 17.34 ± 5.17 and 21.06 ± 8.22, respectively, all $p < .001$). Vessel sharpness was significantly higher for PCD-CT than for EID-CT ($p < .001$).

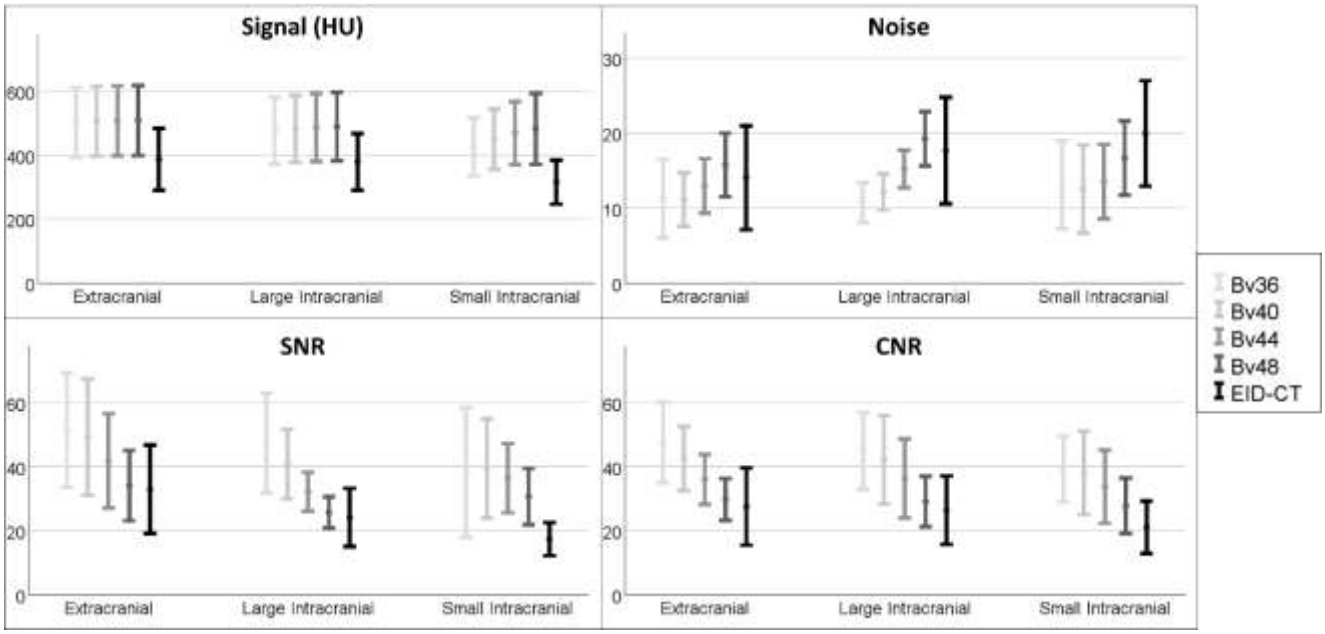

FIG 2. Quantitative image quality analysis. Signal, noise, SNR and CNR scores of the PCD-CT (Bv36, Bv40, Bv44, Bv48) and EID-CT images represented with error bars (means ± SD). (Bv = Body vascular, CNR = Contrast-to-Noise Ratio, EID-CT = Energy-integrating detector CT, HU = Hounsfield unit, PCD-CT = Photon-counting detector CT, SD = Standard deviation, SNR = Signal-to-Noise Ratio)

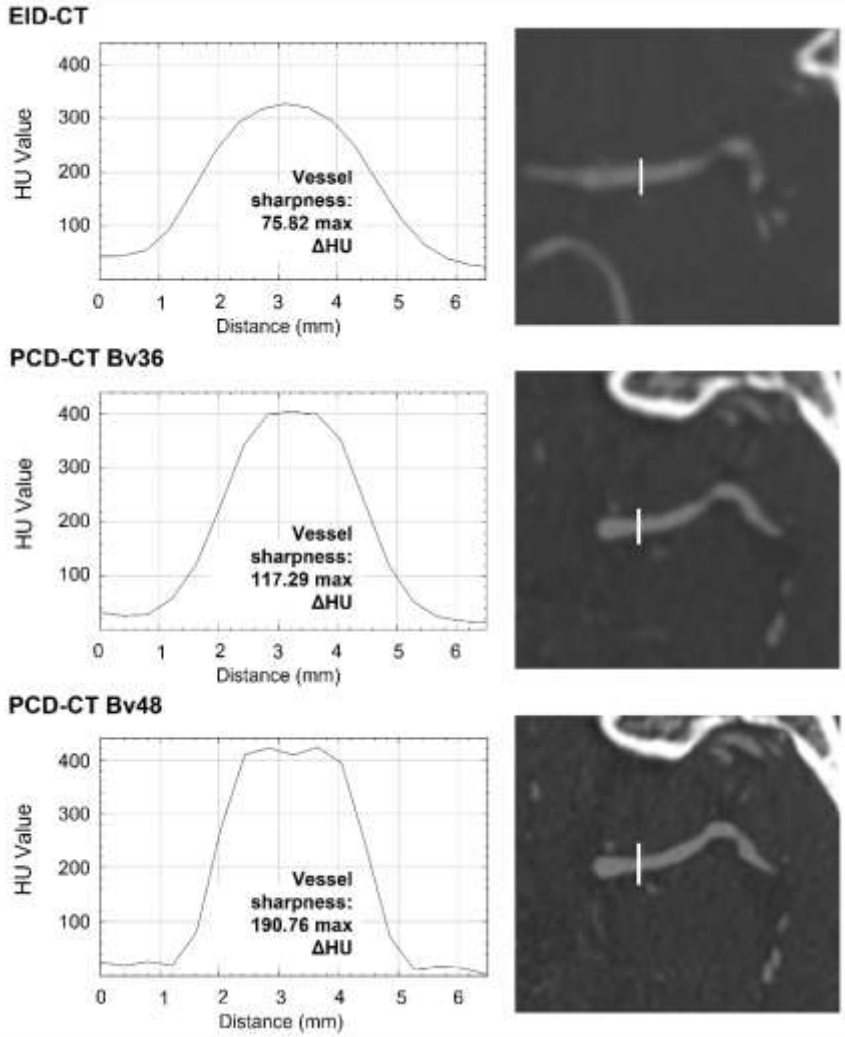

FIG 3. Example of vessels sharpness measurements. Line profiles of the middle cerebral artery and corresponding images: EID-CT (top), PCD-CT Bv36 (middle), PCD-CT Bv48 (bottom). A steeper slope representing sharper vessel wall can be observed in the Bv48 image (vessel sharpness = 217.8 max ΔHU), compared to the Bv36 (vessel sharpness = 139.8 max ΔHU) and the EID-CT image (vessel sharpness = 102.6 max ΔHU). (Bv = Body vascular, EID-CT = Energy-integrating detector CT, HU = Hounsfield unit, PCD-CT = Photon-counting detector CT)

Qualitative Analysis

Moderate agreement ($\alpha = 0.50$) was found between the three readers for qualitative ratings using the 5-point Likert-type scale. The qualitative analysis revealed the superiority of PCD-CT (Bv48) over EID-CT at each intracranial location (all $p < .001$). Images reconstructed with either the Bv44 or Bv48 kernel achieved the highest scores (Figure 4 and Supplementary Table 5). However, the difference between Bv44 and Bv48 was not statistically significant ($p = .166 – 1.00$). When reviewing the PCD-CT images side by side, the Bv48 reconstruction was selected as the most suitable for the evaluation of intracranial aneurysms by the readers in 80% of cases, while Bv44 was chosen in 20% of the cases.

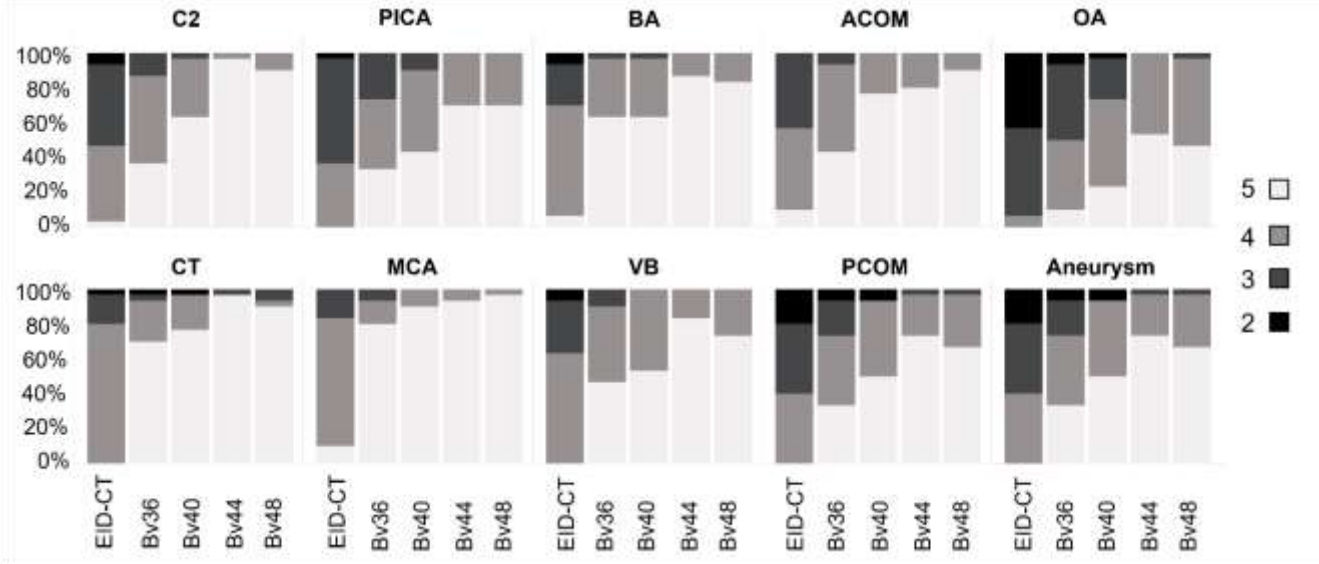

FIG 4. Qualitative image quality scores from the EID-CT and PCD-CT CT (Bv36, Bv40, Bv44, Bv48) images. Stacked bar charts show the pooled ratings from three readers, in percentages. The 10 evaluated intracranial locations: internal carotid artery (C2 segment), posterior inferior cerebellar arteries (PICA), basilar artery (BA), anterior communicating artery (ACOM), ophthalmic arteries (OA), carotid terminus (CT), middle cerebral artery (MCA), vertebral artery – basilar artery junctions (VB), posterior communicating artery (PCOM), and the location of the aneurysm/s. Interpretation of scores: 5 = excellent image quality, 4 = good image quality, 3 = acceptable image quality, 2 = barely satisfactory image quality, 1 = unacceptable image quality. (Bv = Body vascular, EID-CT = Energy-integrating detector CT, PCD-CT = Photon-counting detector CT)

DISCUSSION

The present study evaluated the objective and subjective image quality of UHR PCD-CTA for neurovascular imaging using different levels of kernel sharpness in patients with intracranial saccular aneurysms. Our results highlight the significance of sharper kernels in enhancing the characterization of intracranial aneurysms. The use of the Bv48 kernel significantly increased vessel sharpness, especially of the small intracranial arteries. Our analysis included a comparison of PCD-CT and EID-CT images, confirming previous findings that PCD-CT offers superior image quality for neurovascular imaging.[21, 22] Objectively, UHR (0.2 mm) PCD-CT images significantly increased vessel sharpness and provided improved subjective image quality compared to the standard of care EID-CT. Out of the four reconstruction kernels evaluated on PCD-CT, the three readers of the study favored the sharpest reconstructions kernel for the visualization of saccular aneurysms. Although radiation dose reduction was not the primary focus of this study, our results suggest that improved image quality may be achievable with PCD-CT at a significantly reduced radiation dose compared to EID-CT.

The recent introduction of photon-counting CT into clinical practice promises significant advantages over EID-CT in many diagnostic fields as it offers precise visualization of small anatomic structures and depiction of subtle pathologic changes.[23-26] Moreover, improved lumen visualization and plaque imaging have been reported in various in vitro and in vivo studies, commonly in coronary imaging.[19, 27] As for neurovascular imaging, the image quality of PCD-CTA has been shown to be excellent by using polyenergetic as well as monoenergetic reconstructions.[28, 29]

Related literature on kernel optimization for intracranial aneurysm imaging has been limited to EID-CT platforms. O'Meara et al. showed that higher spatial frequencies and greater image details are more comparable to 3-dimensional rotational angiography utilizing a sharp reconstruction kernel (H60f) in contrast to a smooth kernel (H20f).[18] They report that using a sharper kernel can improve image resolution but may also increase image noise. Nevertheless, this can lead to improved decision-making ability and clinical utility of CTA, by providing more accurate anatomic characterization of intracranial aneurysms. Yang et al. evaluated the image quality of coronary CT angiography using PCD-CT with four kernels sharpness levels (36/40/44/48) across three different kernel types (Br/Bv/Qr).[30] Based on their objective and subjective image quality results, the authors recommended the use of Bv40 for spectral PCD-CT coronary angiography applications. Image quality of PCD-CT for neurovascular applications across different kernel reconstructions requires further determination.

To the best of our knowledge, the present study represents the first systematic assessment of image quality across different reconstruction kernels for neurovascular imaging using PCD-CT. Our preliminary results provide quantitative and qualitative image quality measures of ultra-high-resolution PCD-CT imaging in a selected group of patients with intracranial saccular aneurysms. Our quantitative analysis yielded predictable results, showing that image noise increases by utilizing sharper kernels, resulting in a continuous decrease in

SNR and CNR. Nevertheless, our qualitative image quality analysis demonstrated a clear preference of the readers for the sharpest kernels, outperforming the other PCD-CT reconstructions, as well as the standard of care EID-CT images. The comparison of EID-CT with the Bv48 PCD-CT images revealed that while the Bv48 kernel performs less favorably in quantitative terms compared to other PCD-CT reconstructions, it still demonstrates comparable or superior performance over EID-CT. The utilization of quantitative measures, such as signal, noise, SNR and CNR, offers a robust framework for assessing image quality. However, for a comprehensive evaluation of image quality, both qualitative and qualitative assessments should be taken into account, as they provide complementary information. When in disagreement, the authors of this manuscript argue that qualitative evaluation may outweigh the quantitative evaluation. The Bv44 and Bv48 kernels both delivered superior qualitative image quality. However, the observers favored the Bv48 reconstructions kernel for evaluating the relatively small-sized aneurysms identified in the study cohort, likely due to the improved vessel sharpness, notably observed in the small intracranial arteries.

Intracranial vessel visualization with state-of-the-art EID-CT technology provides good image quality and enables the correct visualization of intracranial aneurysms but usually suffers from limitations in visualizing smaller aneurysms. While digital subtraction angiography remains the "gold standard" test for the detection and characterization of intracranial aneurysms, UHR PCD-CT has the potential to offer less invasive imaging even for small intracranial aneurysms with significantly reduced radiation dose. Our preliminary results may provide a valuable reference to exploit the full potential of the ultra-high-resolution mode of head and neck PCD-CTA.

The limitations of our study merit consideration. First, this preliminary study included a very small number (ten) of patients from a single center, which limits the generalizability of our results. Second, only one type of kernel (Bv) and four levels of kernel sharpness (36, 40, 44, 48) were evaluated on PCD-CT. The Bv (body vascular) is the kernel type routinely used in our institution for head and neck CTA. As we aimed to compare image quality of EID-CT and PCD-CT, we applied a range of reconstructions kernels available on the PCD-CT scanner that are relatively comparable with the reconstruction kernel used for EID-neuro CT angiography in clinical practice at our institution. The Bv48 is the sharpest kernel evaluated in this study, but it is not the sharpest option available on the PCD-CT. Future studies may investigate the highest, limiting level of kernel sharpness that provides the optimal image quality. Third, we utilized QIR at strength level 1 for all PCD-CT reconstructions. However, higher QIR levels could potentially compensate the increase in image noise caused by utilizing sharper kernel levels. Future studies should explore the potential benefits of using sharp kernels in a combination with higher QIR levels to achieve improved image quality. Fourth, ROIs were placed manually by a single observer, which could introduce the risk of measurement bias.

CONCLUSIONS

Our preliminary study shows that UHR PCD-CTA may provide improved image quality for neurovascular imaging applications. A sharper reconstruction kernel seems to be beneficial to achieve optimal image quality for the evaluation of intracranial aneurysms. Further studies are needed to assess the impact of UHR PCD-CT on patient management and outcome.

ACKNOWLEDGMENTS

To all the staff of the Department of Radiology for their technical guidance and contribution to this study and manuscript.

REFERENCES

1. Chen X, Liu Y, Tong H, et al. Meta-analysis of computed tomography angiography versus magnetic resonance angiography for intracranial aneurysm. *Medicine (Baltimore)*, 2018; *97*(20), e10771. https://doi.org/10.1097/md.0000000000010771
2. Ni Q Q, Chen G Z, Schoepf U J, et al. Cerebral CTA with Low Tube Voltage and Low Contrast Material Volume for Detection of Intracranial Aneurysms. *AJNR Am J Neuroradiol*, 2016; *37*(10), 1774-1780. https://doi.org/10.3174/ajnr.A4803
3. Menke J, Larsen J, & Kallenberg K. Diagnosing cerebral aneurysms by computed tomographic angiography: meta-analysis. *Ann Neurol*, 2011; *69*(4), 646-654. https://doi.org/10.1002/ana.22270
4. Westerlaan H E, van Dijk J M, Jansen-van der Weide M C, et al. Intracranial aneurysms in patients with subarachnoid hemorrhage: CT angiography as a primary examination tool for diagnosis--systematic review and meta-analysis. *Radiology*, 2011; *258*(1), 134-145. https://doi.org/10.1148/radiol.10092373
5. Xing W, Chen W, Sheng J, et al. Sixty-four-row multislice computed tomographic angiography in the diagnosis and characterization of intracranial aneurysms: comparison with 3D rotational angiography. *World Neurosurg*, 2011; *76*(1-2), 105-113. https://doi.org/10.1016/j.wneu.2011.01.046
6. Luo Z, Wang D, Sun X, et al. Comparison of the accuracy of subtraction CT angiography performed on 320-detector row volume CT with conventional CT angiography for diagnosis of intracranial aneurysms. *Eur J Radiol*, 2012; *81*(1), 118-122. https://doi.org/10.1016/j.ejrad.2011.05.003
7. Willemink M J, Persson M, Pourmorteza A, et al. Photon-counting CT: Technical Principles and Clinical Prospects. *Radiology*, 2018; *289*(2), 293-312. https://doi.org/10.1148/radiol.2018172656
8. Rajendran K, Petersilka M, Henning A, et al. First Clinical Photon-counting Detector CT System: Technical Evaluation. *Radiology*, 2022; *303*(1), 130-138. https://doi.org/10.1148/radiol.212579
9. Kreisler B. Photon counting Detectors: Concept, technical Challenges, and clinical outlook. *Eur J Radiol*, 2022; *149*, 110229. https://doi.org/10.1016/j.ejrad.2022.110229
10. Benson J C, Rajendran K, Lane J I, et al. A New Frontier in Temporal Bone Imaging: Photon-Counting Detector CT Demonstrates Superior Visualization of Critical Anatomic Structures at Reduced Radiation Dose. *AJNR Am J Neuroradiol*, 2022; *43*(4), 579-584. https://doi.org/10.3174/ajnr.A7452
11. Rajagopal J R, Farhadi F, Solomon J, et al. Comparison of Low Dose Performance of Photon-Counting and Energy Integrating CT. *Acad Radiol*, 2021; *28*(12), 1754-1760. https://doi.org/10.1016/j.acra.2020.07.033
12. Pourmorteza A, Symons R, Henning A, et al. Dose Efficiency of Quarter-Millimeter Photon-Counting Computed Tomography: First-in-Human Results. *Invest Radiol*, 2018; *53*(6), 365-372. https://doi.org/10.1097/rli.0000000000000463
13. Rajagopal J R, Farhadi F, Richards T, et al. Evaluation of Coronary Plaques and Stents with Conventional and Photon-counting CT: Benefits of High-Resolution Photon-counting CT. *Radiol Cardiothorac Imaging*, 2021; *3*(5), e210102. https://doi.org/10.1148/ryct.2021210102
14. Higashigaito K, Mergen V, Eberhard M, et al. CT Angiography of the Aorta Using Photon-counting Detector CT with Reduced Contrast Media

Volume. *Radiol Cardiothorac Imaging*, 2023; *5*(1), e220140. https://doi.org/10.1148/ryct.220140
15. Zhou W, Bartlett D J, Diehn F E, et al. Reduction of Metal Artifacts and Improvement in Dose Efficiency Using Photon-Counting Detector Computed Tomography and Tin Filtration. *Invest Radiol*, 2019; *54*(4), 204-211. https://doi.org/10.1097/rli.0000000000000535
16. Milos R I, Röhrich S, Prayer F, et al. Ultrahigh-Resolution Photon-Counting Detector CT of the Lungs: Association of Reconstruction Kernel and Slice Thickness With Image Quality. *AJR Am J Roentgenol*, 2023; *220*(5), 672-680. https://doi.org/10.2214/ajr.22.28515
17. von Spiczak J, Mannil M, Peters B, et al. Photon Counting Computed Tomography With Dedicated Sharp Convolution Kernels: Tapping the Potential of a New Technology for Stent Imaging. *Invest Radiol*, 2018; *53*(8), 486-494. https://doi.org/10.1097/rli.0000000000000485
18. O'meara B, Rahal J P, Lauric A, & Malek A M. Benefit of a sharp computed tomography angiography reconstruction kernel for improved characterization of intracranial aneurysms. *Neurosurgery*, 2014; *10 Suppl 1*, 97-105; discussion 105. https://doi.org/10.1227/neu.0000000000000167
19. Mergen V, Sartoretti T, Baer-Beck M, et al. Ultra-High-Resolution Coronary CT Angiography With Photon-Counting Detector CT: Feasibility and Image Characterization. *Invest Radiol*, 2022; *57*(12), 780-788. https://doi.org/10.1097/rli.0000000000000897
20. Decker J A, O'Doherty J, Schoepf U J, et al. Stent imaging on a clinical dual-source photon-counting detector CT system-impact of luminal attenuation and sharp kernels on lumen visibility. *Eur Radiol*, 2023; *33*(4), 2469-2477. https://doi.org/10.1007/s00330-022-09283-4
21. Symons R, Reich D S, Bagheri M, et al. Photon-Counting Computed Tomography for Vascular Imaging of the Head and Neck: First In Vivo Human Results. *Invest Radiol*, 2018; *53*(3), 135-142. https://doi.org/10.1097/rli.0000000000000418
22. Pourmorteza A, Symons R, Reich D S, et al. Photon-Counting CT of the Brain: In Vivo Human Results and Image-Quality Assessment. *AJNR Am J Neuroradiol*, 2017; *38*(12), 2257-2263. https://doi.org/10.3174/ajnr.A5402
23. Gaillandre Y, Duhamel A, Flohr T, et al. Ultra-high resolution CT imaging of interstitial lung disease: impact of photon-counting CT in 112 patients. *Eur Radiol*, 2023; *33*(8), 5528-5539. https://doi.org/10.1007/s00330-023-09616-x
24. Prayer F, Kienast P, Strassl A, et al. Detection of Post-COVID-19 Lung Abnormalities: Photon-counting CT versus Same-Day Energy-integrating Detector CT. *Radiology*, 2023; *307*(1), e222087. https://doi.org/10.1148/radiol.222087
25. Sartoretti T, Landsmann A, Nakhostin D, et al. Quantum Iterative Reconstruction for Abdominal Photon-counting Detector CT Improves Image Quality. *Radiology*, 2022; *303*(2), 339-348. https://doi.org/10.1148/radiol.211931
26. Racine D, Mergen V, Viry A, et al. Photon-Counting Detector CT With Quantum Iterative Reconstruction: Impact on Liver Lesion Detection and Radiation Dose Reduction. *Invest Radiol*, 2023; *58*(4), 245-252. https://doi.org/10.1097/rli.0000000000000925
27. Si-Mohamed S A, Boccalini S, Lacombe H, et al. Coronary CT Angiography with Photon-counting CT: First-In-Human Results. *Radiology*, 2022; *303*(2), 303-313. https://doi.org/10.1148/radiol.211780
28. Michael A E, Boriesosdick J, Schoenbeck D, et al. Photon Counting CT Angiography of the Head and Neck: Image Quality Assessment of Polyenergetic and Virtual Monoenergetic Reconstructions. *Diagnostics (Basel)*, 2022; *12*(6). https://doi.org/10.3390/diagnostics12061306
29. Spampinato M V, Rodgers J, McGill L J, et al. Image quality of photon-counting detector CT virtual monoenergetic and polyenergetic reconstructions for head and neck CT angiography. *Clin Imaging*, 2024; *108*, 110081. https://doi.org/10.1016/j.clinimag.2024.110081
30. Yang Y, Fink N, Emrich T, et al. Optimization of Kernel Type and Sharpness Level Improves Objective and Subjective Image Quality for High-Pitch Photon Counting Coronary CT Angiography. *Diagnostics (Basel)*, 2023; *13*(11). https://doi.org/10.3390/diagnostics13111937

SUPPLEMENTAL FILES

Table 1: Acquisition and reconstruction parameters on photon-counting detector CT, and standard of care (SOC) energy-integrating detector CT. (SR = Standard resolution. UHR = Ultra-high resolution).

	Photon-counting detector CT	**Energy-integrating detector CT**
CT Scanner	NAEOTOM Alpha	SOMATOM Force (n=5) SOMATOM go. Top (n=2) SOMATOM Definition Flash (n=1) SOMATOM Emotion 16 (n=1) Revolution CT (n=1)
Iodinated Contrast	80 ml Iohexol (Omnipaque 350 mg/mL)	80 ml Iohexol (Omnipaque 350 mg/mL)
Flow rate	4 – 5 ml/sec	4 – 5 ml/sec
Tube voltage	140 kVp	100 – 140 kVp
Effective mAs[1]	175.70 (± 35.36)	270.22 (± 55.65)
$CTDI_{vol}$ (mGy)	18.87 (± 3.03)	22.55 (±12.16)
Slice thickness (mm)	0.2 (UHR)	0.6 / 0.75 (SR)
Reconstruction kernel	Bv36, Bv40, Bv44, Bv48	Bv36
Iterative reconstruction	1	1

[1] Dose modulation was not utilized in this study.

Table 2. 5-point Likert-type scale used in the qualitative image quality analysis performed by three experienced neuroradiologist.

Score	Interpretation	Comment
1	Unacceptable	Poor image quality, poorly defined anatomic details, high image noise or artifacts, non-diagnostic.
2	Barely satisfactory	Reduced image quality, limitations in anatomic detail, increased image noise or artifacts, impairment of diagnostic confidence.
3	Acceptable	Acceptable image quality for adequate evaluation, the noise or artifact may obscure subtle details, with minimal impairment of diagnostic confidence.
4	Good	Good image quality, clear anatomic details, minor image noise or artifacts, no significant impairment of diagnostic confidence.
5	Excellent	Excellent image quality, distinct anatomic details, no or minimal image noise or artifacts, excellent diagnostic confidence.

Table 3. Details of the aneurysms identified in the study population. (ACOM = anterior communicating artery, cm = centimeter, ICA = internal carotid artery, MCA = middle cerebral artery, PCOM = posterior communication artery)

	Location	Dome height x neck (cm)	Type
Patient 1. Aneurysm 1.	Left MCA bifurcation	0.15 x 0.35	Saccular, wide-neck
Patient 2. Aneurysm 2.	Left MCA bifurcation	0.30 x 0.20	Saccular, wide-neck
Patient 3. Aneurysm 3.	Left PCOM	0.30 x 0.20	Saccular, wide-neck
Patient 4. Aneurysm 4.	Left ophthalmic ICA	0.60 x 0.30	Saccular
Patient 4. Aneurysm 5.	Left MCA bifurcation	0.40 x 0.25	Saccular, wide-neck
Patient 5. Aneurysm 6.	ACOM	0.60 x 0.30	Saccular, bilobed
Patient 5. Aneurysm 7.	Left MCA bifurcation	0.20 x 0.10	Saccular
Patient 6. Aneurysm 8.	Right ophthalmic ICA	0.30 x 0.15	Saccular
Patient 7. Aneurysm 9.	ACOM	0.30 x 0.25	Saccular, bilobed, wide-neck
Patient 8. Aneurysm 10.	Left paraclinoid ICA	0.20 x 0.15	Saccular, wide-neck
Patient 8. Aneurysm 11.	Left cavernous ICA	0.25 x 0.25	Saccular, wide-neck
Patient 9. Aneurysm 12.	Left PCOM	0.25 x 0.20	Saccular, wide-neck
Patient 10. Aneurysm 13.	Left ophthalmic ICA	0.60 x 0.30	Saccular

Table 4. Quantitative image quality measurements of the PCD-CT (Bv36, Bv40, Bv44, Bv48) and EID-CT images. All values are reported as means ± SD. (Bv = Body vascular, CNR = Contrast-to-Noise Ratio, EID-CT = Energy-integrating detector CT, FWHM = full-width-half-maximum, PCD-CT = Photon-counting detector CT, SD = Standard deviation, SNR = Signal-to-Noise Ratio)

	Bv36	Bv40	Bv44	Bv48	EID-CT	*p* (Bv36 vs Bv48)	*p* (Bv48 vs EID-CT)
Extracranial arteries							
Signal	516.13 (± 108.10)	519.65 (± 108.70)	521.63 (± 108.72)	521.92 (± 108.53)	387.00 (± 96.17)	**.048**	**< .001**
Noise	11.32 (± 4.97)	11.28 (± 3.39)	13.20 (± 3.50)	16.26 (± 4.36)	14.04 (± 6.94)	**< .001**	.224
SNR	51.68 (± 17.10)	49.43 (± 17.17)	41.80 (± 13.88)	33.83 (± 10.46)	32.88 (± 13.86)	**< .001**	.732
CNR	49.48 (± 12.64)	45.96 (± 13.57)	39.23 (± 11.69)	31.26 (± 7.40)	27.57 (± 12.09)	**< .001**	.656
Sharpness	158.44 (± 40.89)	179.76 (± 46.97)	212.82 (± 57.77)	234.41 (± 64.07)	95.80 (± 25.05)	**< .001**	**< .001**
FWHM	4.16 (± 0.64)	4.19 (± 0.64)	4.18 (± 0.62)	4.19 (± 0.61)	4.34 (± 1.00)	.163	.642
Large intracranial arteries							
Signal	476.88 (± 104.70)	482.025 (± 104.82)	486.43 (± 106.03)	489.38 (± 106.88)	379.58 (± 88.82)	**.008**	**.004**
Noise	10.70 (± 2.69)	12.15 (± 2.39)	15.20 (± 2.50)	19.25 (± 3.62)	17.65 (± 7.12)	**< .001**	.646
SNR	47.39 (± 15.68)	40.85 (± 10.92)	32.21 (± 6.09)	25.71 (± 4.85)	24.13 (± 9.09)	**< .001**	.494
CNR	44.98 (± 12.06)	42.23 (± 13.86)	36.36 (± 12.38)	29.10 (± 7.88)	26.40 (± 10.71)	**< .001**	.464
Sharpness	140.40 (± 36.72)	157.02 (± 40.23)	183.26 (± 48.07)	202.67 (± 53.43)	99.34 (± 21.75)	**< .001**	**< .001**
FWHM	3.88 (± 0.65)	3.89 (± 0.63)	3.88 (± 0.62)	3.88 (± 0.61)	4.01 (± 0.81)	.879	.510
Small intracranial arteries							
Signal	425.74 (± 91.21)	449.54 (± 94.21)	469.15 (± 98.15)	482.23 (± 110.89)	315.39 (± 68.89)	**< .001**	**< .001**
Noise	13.09 (± 5.86)	12.52 (± 5.90)	13.51 (± 4.98)	16.66 (± 4.96)	19.95 (± 7.04)	**< .001**	**.012**

SNR	38.24 (± 20.32)	39.44 (± 15.49)	36.47 (± 10.84)	30.65 (± 8.86)	17.34 (± 5.17)	.228	**< .001**
CNR	39.29 (± 10.36)	38.09 (± 13.09)	33.80 (± 11.47)	27.76 (± 8.71)	21.06 (± 8.22)	**< .001**	**< .001**
Sharpness	139.87 (± 31.23)	163.80 (± 36.29)	197.02 (± 43.85)	221.69 (± 49.46)	94.03 (± 19.41)	**< .001**	**< .001**
FWHM	2.23 (± 0.28)	2.18 (± 0.32)	2.13 (± 0.35)	2.10 (± 0.37)	2.60 (± 0.38)	**< .001**	**< .001**

Table 5. Qualitative image quality scores of the PCD-CT (Bv36, Bv40, Bv44, Bv48) and EID-CT images. Three readers independently rated the images on a 5 point Likert-type scale (5=excellent image quality, 1= Unacceptable image quality) at 10 intracranial locations: internal carotid artery (C2 segment), posterior inferior cerebellar arteries (PICA), basilar artery (BA), anterior communicating artery (ACOM), ophthalmic arteries (OA), carotid terminus (CT), middle cerebral artery (MCA), vertebral artery – basilar artery junctions (VB), posterior communicating artery (PCOM), and the location of the aneurysm/s. All values are reported as means ± SD. A p less than .05 was considered statistically significant. (Bv = Body vascular, CNR = Contrast-to-Noise Ratio, EID-CT = Energy-integrating detector CT, PCD-CT = Photon-counting detector CT, SD = Standard deviation, SNR = Signal-to-Noise Ratio)

	PCD-CT				**EID-CT**	*p*	*p*
	Bv36	**Bv40**	**Bv44**	**Bv48**		**Bv44 vs Bv48**	**Bv48 vs EID-CT**
C2	4.23 (± 0.68)	4.60 (± 0.56)	4.97 (± 0.18)	4.90 (± 0.30)	3.43 (± 0.68)	.314	**<.001**
PICA	4.07 (± 0.79)	4.33 (± 0.66)	4.70 (± 0.47)	4.70 (± 0.47)	3.33 (± 0.55)	1.00	**<.001**
BA	4.60 (± 0.56)	4.60 (± 0.56)	4.87 (± 0.35)	4.83 (± 0.38)	3.70 (± 0.70)	.655	**<.001**
ACOM	4.37 (± 0.62)	4.77 (± 0.43)	4.80 (± 0.41)	4.90 (± 0.31)	3.67 (± 0.66)	.166	**<.001**
OA	3.53 (± 0.78)	3.93 (± 0.79)	4.53 (± 0.51)	4.43 (± 0.57)	2.63 (± 0.62)	.634	**<.001**
CT	4.60 (± 0.72)	4.70 (± 0.65)	4.93 (± 0.37)	4.83 (± 0.53)	3.77 (± 0.50)	.360	**<.001**
MCA	4.73 (± 0.58)	4.90 (± 0.31)	4.93 (± 0.25)	4.97 (± 0.18)	3.93 (± 0.52)	.634	**<.001**
VB	4.37 (± 0.67)	4.53 (± 0.51)	4.83 (± 0.38)	4.73 (± 0.45)	3.57 (± 0.63)	.166	**<.001**
PCOM	4.00 (± 0.91)	4.37 (± 0.81)	4.70 (± 0.54)	4.63 (± 0.56)	3.20 (± 0.76)	.314	**<.001**
Aneurysm	4.17 (± 0.70)	4.57 (± 0.57)	4.80 (± 0.48)	4.83 (± 0.38)	3.50 (± 0.78)	.564	**<.001**